Volumetry of Temporopolar, Perirhinal, Entorhinal and Parahippocampal Cortex from High-resolution MR Images: Considering the Variability of the Collateral Sulcus

Jens C. Pruessner[1,2], Stefan Köhler[3], Joelle Crane[1], Marita Pruessner[1,2], Catherine Lord[1,2], Andrea Byrne[1], Noor Kabani[1,4], D. Louis Collins[1] and Alan C. Evans[1]

[1]McConnell Brain Imaging Center, Montreal Neurological Institute, [2]Douglas Hospital Research Center, McGill University, Montreal, Quebec, Canada, [3]Department of Psychology, University of Western Ontario, London, Ontario and [4]Bloomfield Centre for Aging, Lady Davis Institute, McGill University, Montreal, Quebec, Canada

Researchers in clinical and basic neuroscience frequently target structures of the human medial temporal lobe (MTL) for volumetric analysis with magnetic resonance imaging (MRI). In neurodegenerative diseases, a precise volumetric analysis of MTL structures can assist in differential diagnosis and can be used in guiding early treatment. Also, in functional neuroimaging, exact localization is crucial for the correct interpretation of focal MTL activations with respect to specific memory functions. In presently available protocols, precise and consistent volumetric analysis of MTL structures is compromised in numerous ways. Most importantly, in order to cover all structures of the MTL, the researcher is presently forced to combine independently developed segmentation protocols for different structures from different laboratories. This approach limits anatomical precision because these protocols are based on different anatomical guidelines and descriptions that cannot easily be integrated. The segmentation approach presented in this paper was designed to address this issue by presenting segmentation guidelines for all major structures of the parahippocampal gyrus (PHG). It was developed directly to complement a volumetric protocol for hippocampus and amygdala (Pruessner *et al*., 2000, Cereb Cortex 10:433–442), thus allowing volumetric assessment of all major MTL structures in an integrated and consistent manner. Furthermore, it takes into consideration the neuroanatomical appearance of the collateral sulcus by presenting a method to correct the volumes of the surrounding cortices for the variability of this sulcus. The protocol was validated using MR images of 40 healthy normal control subjects (20 men and 20 women, age range 18–42 years). Intra- and interrater coefficients are presented, together with mean values for the volumes of all PHG structures, correlations with age and sex, and tests for hemispheric differences.

Introduction

Research in neuropsychology and functional neuroimaging has firmly established that the human medial temporal lobe (MTL) plays an important role in the acquisition and retention of information from memory (Schacter and Wagner, 1999; Scoville and Milner, 2000). Neuroanatomical investigations have shown that the MTL of human and non-human primates is not a homogeneous region, but consists of several different structures that can be distinguished based on histological patterns and on their connectivity with other regions (Amaral and Insausti, 1990). It is comprised of allo- and subcortical structures such as the hippocampus and amygdala, as well as neocortical structures including temporopolar cortex (TPC), perirhinal cortex (PRC), entorhinal cortex (EC) and parahippocampal cortex (PHC; sometimes also referred to as ectorhinal cortex). Together, these neocortical structures make up the parahippocampal gyrus (PHG). While the general involvement of the MTL region in memory functions is well documented (Cabeza and Nyberg, 2000), recent research has also started to investigate whether individual structures in this region may serve unique memory functions that, although related, can to some extent be dissociated and defined independently (Eichenbaum *et al.*, 1994; Aggleton and Brown, 1999). Most of this work in humans has relied on functional neuroimaging. Here, the exact delineation of the individual structures in the subjects under study is essential in order to allocate specific memory functions to specific structures (Gabrieli *et al.*, 1997; Stark and Squire, 2001).

In clinical neuroscience, it has been recognized that MTL structures are involved in neurological disease states such as Alzheimer's, Parkinson's, schizophrenia and temporal lobe epilepsy (Double *et al.*, 1996; Mori *et al.*, 1997; Bernasconi *et al.*, 2001). Investigation of these structures with magnetic resonance imaging (MRI) has assisted clinicians with the initial diagnosis and allowed them to follow volume changes associated with the progression of these diseases. In addition, methods employing voxel-based regression models have demonstrated changes in morphometry of these structures in relation to specific neurodegenerative diseases (Baron *et al.*, 2001). All of these applications require accurate, precise and reliable anatomical descriptions and segmentation protocols for the assessment of MTL volumes. Unfortunately, the segmentation protocols currently available for the assessment of different structures of the MTL do not satisfy this need, for a number of reasons.

First, none of the currently available protocols provides guidelines for the volumetric analysis of all MTL structures, forcing the researcher to combine different protocols when examining various structures in the same study. This is unsatisfactory because different protocols use different anatomical definitions for the descriptions of specific structures.

Secondly, anatomical variations of the PHG across individuals cause considerable variability of shape and size of its cortices, making an exact description difficult. The one structure that adds most to the variability of the different cortices in the PHG is the collateral sulcus (CS), which can show significant variations in length, depth and number of branches across subjects. Because the EC, PRC and PHC are located along the medial and lateral bank of this sulcus, variations in the CS have profound effects on the volume and size of these cortices, regardless of any disease state. One of the segmentation protocols available has taken these variations into account by presenting modified segmentation guidelines for each of the anatomical aberrations (Insausti *et al.*, 1998). However, if these variations are not further considered in the statistical analysis, these modified guidelines lead to increased intragroup variability in volumetric measurements, a point that was acknowledged by the authors.

Thirdly, differences in acquisition protocols and image processing also add to the variability of volumetric measurements obtained with different segmentation protocols. These differences can occur as a result of different field strengths of the employed MR scanners, different acquisition sequences and differences in the standardization of images. Most of the protocols currently available employ the method of correcting all

of their individual structures for total intracranial volume (Kesslak *et al.*, 1991; Krasuski *et al.*, 1998; Killiany *et al.*, 2000). Unfortunately, in the absence of a standardized method for calculating intracranial volume, variations in the implementation of this procedure can be expected to result in variations in measurements across laboratories. Some groups perform a transformation of MR images into standardized stereotaxic space, a common procedure in functional imaging (Bernasconi *et al.*, 1999, 2000), before conducting volumetric analyses. This should perhaps be regarded as the best available method for standardization, since it is reliable, validated, reproducible and greatly facilitates the analysis by presenting the researcher with a standardized brain size for all MR images.

Finally, differences can emerge from the visualization software, with some laboratories being restricted to a single orientation and limited magnification capabilities for manual segmentation (Barta *et al.*, 1997), while others make use of multiplanar images with unlimited magnification (Honeycutt *et al.*, 1998). The differences resulting from viewing structures in different angles with different magnifications further add to the variability in measurements obtained with different protocols.

The protocol introduced in the present paper was developed to overcome many of the problems listed when measuring the major PHG structures. It combines precise anatomical descriptions with clear rules for segmentation and takes advantage of advanced visualization software providing multiple image planes. The protocol is based on anatomical landmarks that were published previously and were derived from a combination of MRI and histological data (Insausti *et al.*, 1998). In addition, it offers a new method to correct the volumes of EC, PRC and PHC for the variability of the CS, which can add important information on MTL structures. Finally and perhaps most importantly, the protocol was developed directly to complement a previously published segmentation protocol for the volumetric assessment of the hippocampus and amygdala (Pruessner *et al.*, 2000). When combined, these two protocols allow for a thorough examination of all major MTL structures in an integrated manner with consistent neuroanatomical definitions.

Materials and Methods

Subjects and Sociodemographic Assessment

A total of 40 brain volumes (acquired from 20 female and 20 male subjects) was employed for this study. All recruited subjects were screened for the absence of physical illnesses, medical conditions and history of neurological or psychiatric diseases (Giedd *et al.*, 1996a,b). Subjects were in early adulthood, between 18 and 42 years of age (mean age 25.45 ± 5.4 years). All subjects were right-handed.

MR Image Acquisition

The scans were collected as part of the ongoing 'International Consortium of Brain Mapping' (ICBM) initiative to create a statistical atlas of the normal adult brain (Mazziotta *et al.*, 1995). This protocol generates T_1-, T_2- and PD-weighted image volumes with a slice separation of 1 mm for the T_1-weighted images. For the purpose of the study, only the T_1-weighted images were employed. The T_1 volumes were acquired using a three-dimensional (3D) spoiled gradient echo acquisition with sagittal volume excitation (T_R = 18, T_E = 10, flip angle = 30°, 140 1 mm contiguous sagittal slices). The rectangular field of view (FOV) for the sagittal images was 256 mm (SI) × 204 mm (AP).

MR Image Analysis

All images were transferred to a network of Silicon Graphics workstations (Silicon Graphics, Mountain View, CA). Several algorithms were used consecutively to prepare the images for manual segmentation. This included correction for magnetic field non-uniformities (Sled *et al.*, 1998), linear stereotaxic transformation (Collins *et al.*, 1994) into coordinates based on the Talairach atlas (Talairach and Tournoux, 1988) and resampling onto a 1 mm voxel grid before image segmentation using a linear interpolation kernel. It has been shown that the automatic stereotaxic transformation is as accurate as the manual procedure but shows higher stability (Collins *et al.*, 1994). Also, the correction for image intensity has been proven to recover most of the image artifacts present in the ICBM MR database (Sled *et al.*, 1998).

Volumetric analysis was performed with the interactive software package DISPLAY developed at the Brain Imaging Center of the Montreal Neurological Institute. This program allows simultaneous viewing and segmentation of volumes in coronal, sagittal and horizontal orientations. Additionally, the user can define angles for viewing of images that are presented in a fourth window. This allows the user to view coronal slices simultaneously along the AC–PC line and the line perpendicular to the long axis of the HC, which has been suggested to result in superior visualization of the target structures in the MTL for segmentation (de Leon *et al.*, 1997). In addition, the CS can be better visualized when the image is displayed in plane with the sulcus. The program accommodates labeling of structures in all orientations. Labeled structures in the three standard orientations immediately appear in all shown orientations. Due to the contiguous 1 mm slices, the investigator can navigate through the brain in 1 mm intervals in coronal, sagittal and horizontal orientations. Volumes of labeled structures are calculated automatically by the software. Regions of interest can be edited manually and semiautomatically by thresholding the image. The program further allows rendering of segmented areas for 3D visualization of specific structures.

Gross Overview of MTL Neuroanatomy

The TPC, EC, PRC and PHC are located on the inferomedial surface of the temporal lobe along a large portion of its rostrocaudal extent. The TPC extends from the temporal pole to the rostral beginning of the CS, or the first appearance of the frontotemporal junction (FTJ), depending on which of these structures is located further anterior in the individual subject. The transition between TPC and PRC usually coincides with the first appearance of the amygdala. The PRC extends from the first appearance of the CS (or the FTJ) to a level slightly posterior to the disappearance of the gyrus intralimbicus of the hippocampus. The EC is embedded in the PRC on the medial side and usually starts a few millimeters posterior to the first appearance of the PRC and ends a few millimeters anterior to the end of it. Posterior to the PRC and EC, the PHC covers the caudal part of the PHG from approximately the level of the gyrus intralimbicus to the posterior end of the hippocampus (Fig. 1).

Segmentation of the MTL

An overview of the measured MTL structures and their definitions for segmentation is presented in Table 1. The structures described in this protocol were segmented by selecting the coronal view and moving from the frontal pole of the temporal lobe posterior to the end of the hippocampal tail. Frequent references to other planes were made to gain clarity about the exact location of individual cortices or sulci, although in general the labeling was performed in the coronal view. While all cortices visible in the coronal view were labeled simultaneously, the CS was demarcated prior to the other MTL structures in order to facilitate the

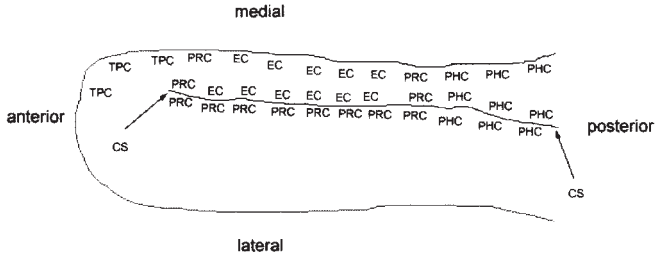

Figure 1. Schematic view of the MTL, shown from inferior perspective in a horizontal orientation cut along the CS. Other sulci of the MTL have been omitted to improve visualization. The location of the different cortices of the MTL as defined in the current protocol can be deduced in reference to the appearance of the CS. Also for reasons of clarity, the collateral sulcus is shown uninterrupted and without side branches.

Table 1
Segmentation guidelines for the MTL structures

Structure	Anterior border	Posterior border	Medial border	Lateral border	Comments
Temporo-polar cortex (TPC)	Temporal pole	Depends on the anterior border of the perirhinal cortex, see below. Special attention has to be given to the superior border of the TPC in its posterior portion; if the gray matter at this point is already perforated due to the imminent appearance of the FTJ, then the most medial aspect of the PHG is the superior border of the TPC	Only exists if the gray matter in the superolateral part of the TPC is already perforated; in this case, the most medial aspect of the PHG is employed as medial border of the TPC	For the first six to ten slices, the TPC is labeled to the midpoint of its mediolateral extent; these borders are then replaced by: (i) the first appearance of the temporopolar sulcus (and thus, the gyrus of Schwalbe) superolateral; and (ii) the inferior temporal or occipitotemporal sulcus inferolateral	Only the medial part of the TPC is segmented
Perirhinal cortex (PRC)	Depends on the length of the collateral sulcus (CS); if CS stretches further anterior than the FTJ, then anterior tip of the CS is the anterior border of the PRC. If CS is shorter or as long than the FTJ, then 1 mm (one slice) anterior to the FTJ is the anterior border of the PRC	Four millimeters posterior to the disappearance of the gyrus intralimbicus, which is 2 mm posterior to the disappearance of the EC (see there)	Before the appearance of the EC: imaginary extension of white matter inferior to the pyriform gyrus; if the amygdala is present, employ the white matter extension of amygdala; if EC is present, the midpoint of the medial bank of the CS; if two CS are present, take the midpoint of the more medial bank	In the most rostral extent, sometimes no CS is present; here, the PRC extends to the fundus of the inferior temporal sulcus or occipitotemporal sulcus, whichever is visible (same as TPC). If one CS is present, then the lateral border is the lateral edge of the lateral bank of this CS; if two CS are present, the lateral border is the fundus of the more lateral CS	Definition of the FTJ: white matter connection between the temporal and frontal lobes; use a threshold defined by the signal intensity in the anterior commissure to determine the first slice making that connection
Entorhinal cortex (EC)	Depends on the extent of the CS; if CS extends further anterior than FTJ, then anterior border is 2 mm posterior to FTJ; if the CS is shorter than the FTJ, then the anterior border of the CS is the rostral extreme of the EC	Two millimeters posterior to the disappearance of the gyrus intralimbicus	Possible medial borders: most medial point of the temporal cortex; amygdala if present; hippocampus if present (excluding subiculum)	ALWAYS the midpoint of the medial bank of the first appearing CS	If CS is interrupted, indicate CS with one voxel to be able to delineate EC and PRC borders; extend CS from anterior and posterior slices to find most likely position of CS in the current slice
Parahippocampal cortex (PHC)	Five millimeters posterior to the disappearance of the gyrus intralimbicus	Last slide in ACPC orientation where the hippocampus can be identified inferomedial to the trigone of the lateral ventricle	For the first four to six slices, the hippocampus (excluding subiculum) marks the superiomedial border. If calcarine sulcus is present, the inferior edge of the calcarine sulcus is medial border	Same as PRC: if one CS is present, the lateral edge of the lateral bank of the CS; if two CS are present, take the fundus of the more lateral CS	

subsequent localization of the cortices. The borders and anatomical landmarks used for the definition of the individual cortices were adapted from the protocol presented by Insausti *et al*. (Insausti *et al.*, 1998) because these had been derived from histological data. The description of the structures in this protocol assumes familiarity with the protocol recently presented by this laboratory (Pruessner *et al.*, 2000) for segmentation of the hippocampus and amygdala.

The segmentation of MTL structures in the current protocol is outlined in three consecutive steps. First, the identification of the FTJ is described. Next, the delineation and segmentation of the CS along its rostrocaudal extent is presented, together with the identification of side branches or interruptions. Lastly, following the temporal lobe from the temporal pole to the posterior end of the tail of the hippocampus in coronal views, the labeling of the individual cortices is shown.

Identification of the FTJ

The white-matter connection between the frontal and temporal lobe is referred to in this protocol as FTJ, but terms such as temporal stem, limen insulae, or temporal incisura can also be found. The FTJ is an important landmark for the identification of medial temporal lobe structures. For its consistent definition across subjects, we determined a signal-intensity value that could serve as a threshold to distinguish white matter from other tissue. We selected this threshold to equal a value that was 10% below the highest MR signal found in the medial part of the anterior commissure (AC). The correction for field-nonuniformities applied to all images prior to segmentation guaranteed the exclusion of inter-hemispheric differences due to signal drift in this approach. To localize the FTJ, the signal intensity of the area between the frontal and temporal lobe was compared to this white-matter threshold in the coronal slices just anterior to where the first appearance of the FTJ was suspected. Moving posterior, the first slice on which the signal intensity in this area exceeded the threshold was defined to mark the first appearance of the FTJ (Fig. 2). In order to overcome the problem of spurious individual signal spikes, the specified signal intensity had to be present in at least eight contiguous voxels to qualify as FTJ connecting the frontal and temporal lobes.

Segmentation of the CS

Since the localization of all structures measured in this protocol critically depends on the location and shape of the CS, special emphasis was put on its reliable identification and demarcation. To ensure this, a series of distinct steps was applied to all MR images containing CS.

First, a coronal slice was chosen in the posterior portion of the hippocampus where the CS was well visible in a location inferomedial to the hippocampus. The correct detection of the CS was confirmed by identifying the adjacent sulci, i.e. the occipitotemporal sulcus, the inferior temporal sulcus and the superior temporal sulcus. If this approach did not allow for easy demarcation of the CS due to the presence of a side branch, a connection with adjacent sulci, or an interruption of the CS, another point in the posterior portion of the hippocampus was chosen, at a distance of at least 10 mm anterior or posterior to the first location. If that image did not allow easy identification of the CS either, yet another slice was chosen until the CS could be identified reliably on at least one coronal slice. The CS was then labeled from its fundus to the cortical surface in this slice (Fig. 3*A*). Regardless of the actual thickness of the CS in the MR image, the sulcus was always labeled with a width of one

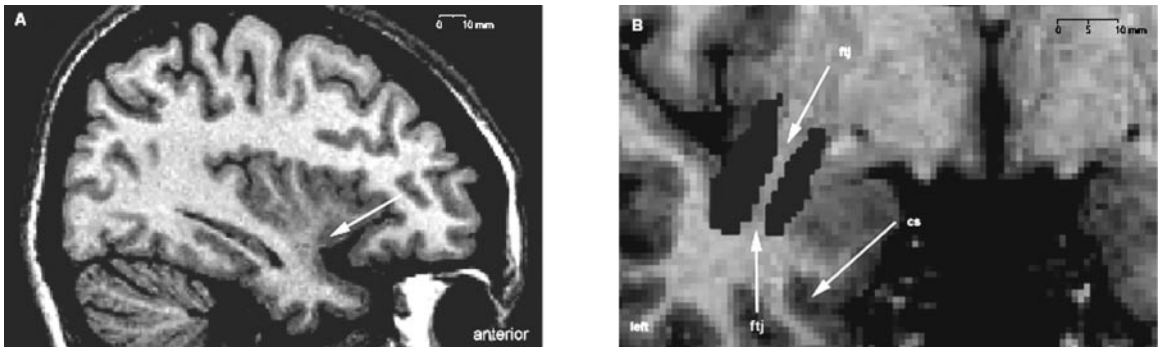

Figure 2. Sagittal (*A*) and coronal (*B*) sections showing a typical FTJ. Once the FTJ was localized by approximation in a sagittal section, its exact presence was confirmed using the segmentation tool and the threshold determined in relation to the AC.

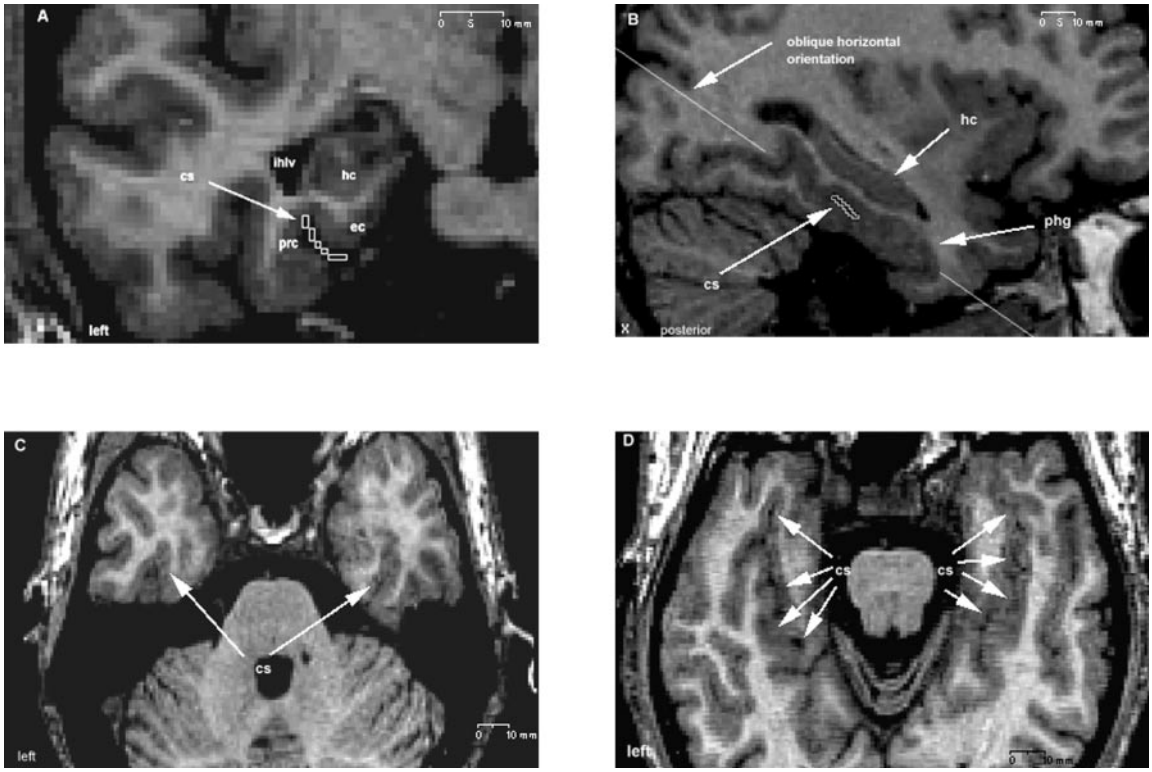

Figure 3. Segmentation of the CS. In a first step, a coronal slice along the rostrocaudal extent of the hippocampus was chosen where the CS was clearly visible and could be separated from the other sulci of the MTL. In this view, the CS was then labeled from the fundus to the surface (*A*). Switching to the sagittal view, the CS was followed and labeled as far as it was visible along its rostrocaudal extent (*B*). The horizontal view cut along the AC-PC line (*C*) or along the long axis of the hippocampus (*D*) in plane with the CS was then added to help in identifying the rostrocaudal extent of the CS.

voxel. Secondly, the resulting label was used in the sagittal view to follow and guide further labeling of the CS along its rostrocaudal extent as far as it was visible in this particular image (Fig. 3*B*). Thirdly, at the level of the most anterior labeled part of the CS in the sagittal view, the CS was examined in the coronal orientation again. The CS was labeled from fundus to cortical surface at this level. Fourthly, labeling of the CS in the coronal view resulted in more anterior and more posterior portions of the CS becoming visible in the sagittal view; these portions were labeled rostrocaudal (in the sagittal view) as they became visible. Segmentation of the CS in coronal and sagittal views was alternated several more times, allowing the delineation of the CS throughout its complete rostrocaudal extent. Notably, this procedure included labeling the CS along its depth from fundus to cortical surface in all coronal slices.

Additional steps were introduced into the protocol to determine the exact rostral extent of the CS, since this is crucial for defining the anterior extent of the PRC and of the EC. Two criteria were introduced that had to be met by the CS at this point:

1. the sulcus had to have a depth of at least 4 mm (for the 1 mm pixels used in this protocol, this measure translated to 4 horizontal or vertical pixels, or 2.5 diagonal pixels);
2. the sulcus had to be surrounded by a semicircle or circle of gray matter forming the surrounding gyrus.

Regarding the caudal end of the CS in the current protocol, segmentation was continued to the level at which the hippocampus was no longer visible. Although the CS does proceed further caudally than the posterior end of the hippocampus, further demarcation was not required here due to the caudal border employed for the PHC (see below).

If an interruption or side branch of the CS was suspected, transverse

views were employed for validation. Here, in an additional display window, an oblique transverse section of the MTL was realigned along the long axis of the CS (angle of orientation shown in Fig. 3*B*) and investigated together with the transverse view parallel to the AC–PC line (Fig. 3*C*,*D*). An interruption, a connection with the occipitotemporal sulcus, or the occurrence of a side branch could usually be validated in these views. In the event of a connection of the CS with the occipitotemporal sulcus, a decision had to be made as to how far the connecting sulcus could be considered a side branch of the CS; it was decided that the side branch had to be <10 mm apart from the main sulcus and had to surface together with the main sulcus in the medial part of the temporal cortex in order to be considered part of the CS. If either or both of these conditions were no longer fulfilled, the sulcus was considered occipitotemporal sulcus.

Finally, in the case of an interruption of the CS, the oblique transverse view was employed to ensure that the slice on which the CS first reappeared was identified correctly. In the slices in which no CS was apparent, the presence of the CS was marked in the area where it appeared in adjacent slices by labeling one pixel in the coronal view. This extrapolation was necessary to allow for continuous segmentation of all MTL structures that normally surround the CS.

Segmentation of medial TPC

The segmentation of the TPC started from the rostral end of the temporal pole and proceeded caudally. The TPC starts to appear in coronal slices inferolateral to the frontal lobe as an ovoid mass of gray matter, with the foldings of the gyri and sulci of the temporal lobe appearing almost immediately. Prior to the appearance of the gyrus of Schwalbe and the inferior or superior temporal sulcus, the medial half of the visible gray matter was included in the TPC. In this section of the TPC, the lateral borders were chosen at the midpoint of the mediolateral extent of the MTL, at the superior and inferior surface. Usually after proceeding four to six slices caudally from the temporal pole, the gyrus of Schwalbe appeared together with the temporopolar sulcus and the inferior or the superior temporal sulcus. These pairs of structures marked the lateral borders of the TPC, with the gyrus of Schwalbe being employed as the superolateral border and the superior or inferior temporal sulcus as inferolateral border. More specifically, since the gyrus of Schwalbe only appears in conjunction with the temporopolar sulcus, the fundus of this sulcus marked the superolateral border of the TPC. For the inferolateral border, if both the superior temporal sulcus and inferior temporal sulcus were present, then the border was defined at the medial edge of the inferior temporal sulcus. If only one of them was present, the medial edge of this sulcus was selected to mark the inferolateral border regardless of the sulcus' identity. If only one landmark was present altogether (the gyrus of Schwalbe dorsally, or the superior or inferior temporal sulcus ventrally), then the second border was defined at the midpoint of the opposite (ventral or dorsal) side (Fig. 4*A*). Finally, if two gyri of Schwalbe were present (in at least two consecutive images), then the more lateral gyrus (i.e. the fundus of the more lateral temporopolar sulcus) was chosen to mark the superolateral border for the TPC (Fig. 4*B*).

Segmentation of PRC

The rostral end of the PRC was identified at the rostral end of the CS or at the FTJ, depending on which of these distinct anatomical landmarks was located further anterior in the individual brain. Usually, the appearance of the CS and the FTJ coincided with the first appearance of the amygdala in the superomedial aspect of the MTL. If the CS proceeded further anterior than the FTJ, then the rostral end of the CS was defined to mark the anterior border of the PRC. If the CS began at the same rostrocaudal level or further caudally than the FTJ, then the rostral end of the PRC was defined as being 1 mm anterior to the FTJ.

The superomedial border in the most anterior portion of the PRC was defined at the most medial aspect of the PHG, at the point where an imaginary extension of the white matter bordering the inferior aspect of the more superior located cortex would touch the pial surface. The gray matter superior to this point was excluded from the PRC, assuming that it represented pyriform cortex. In slices where the amygdala was already present, the more lateral parts of the PRC came close to the inferomedial border of the amygdala. However, usually no direct connection at the inferior and lateral border with the amygdala was present; either a white-matter band or the presence of the sulcus semiannularis delineated the two structures (Fig. 5*A*). In MR images where neither the white-matter band nor the sulcus semiannularis were visible, one row of pixels of gray matter was excluded to distinguish the PRC from the amygdala or pyriform gyrus and to account for partial volume effects. The inferolateral border of the PRC depended on the presence of the CS. If no CS was present in the most rostral part of the PRC, then it extended to the fundus of the inferior temporal sulcus or superior temporal sulcus, depending on which structure was visible. If one CS was present, then the lateral border of the PRC was defined at the edge of the lateral bank of the CS (Fig. 5*B*). In the cases where two CS were present, the lateral border of the PRC was defined at the fundus of the more lateral CS, in accordance with the protocol provided by Insausti *et al* (Insausti *et al*., 1998). The caudal end of the PRC was defined in relationship to the caudal end of the EC (see below).

Segmentation of the EC

The EC is located inferior to the amygdala and remaining pyriform cortex, and superior to the CS and the PRC. The border of the rostral end of the EC also depended on the length of the CS. In cases where the CS stretched further anterior than the FTJ, the rostral end was determined to be 2 mm posterior to the first appearance of the FTJ. If the CS appeared shorter than the FTJ, then the anterior border of the EC was defined at the rostral end of the CS. Superomedially, the EC bordered with the inferomedial portion of the amygdala, if visible. If the amygdala was not yet visible, the white-matter surface of the EC was extended superomedially to help define a virtual border between the EC and the gray-matter structures lying superior. If the sulcus semiannularis was present, then its fundus was chosen as superomedial border of the EC. The EC proceeded ventrally to the CS, where it bordered with the PRC. Its ventrolateral border was always defined at the midpoint of the medial bank of the CS. More dorsally, the transition between gray and white matter marked the lateral border of the EC. Medially, the transition between gray matter and

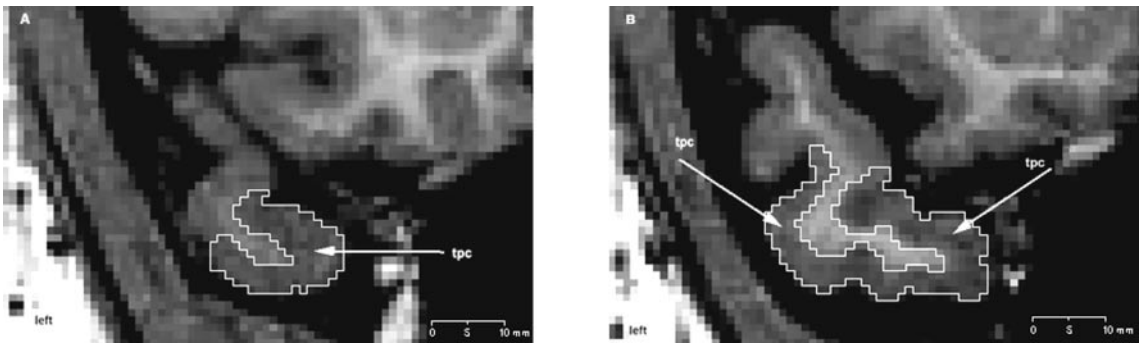

Figure 4. Segmentation of the medial TPC. In the anterior sections of the TPC, when the inferior temporal sulcus (ITS) was not yet visible, only the medial section was segmented, using the midpoint between the mediolateral extent of the TPC as an arbitrary landmark (*A*). In sections further anterior, when the ITS became clearly visible, the ITS was used instead (*B*). The gyrus of Schwalbe (GS) could be used consistently as the superolateral border of the TPC in all subjects.

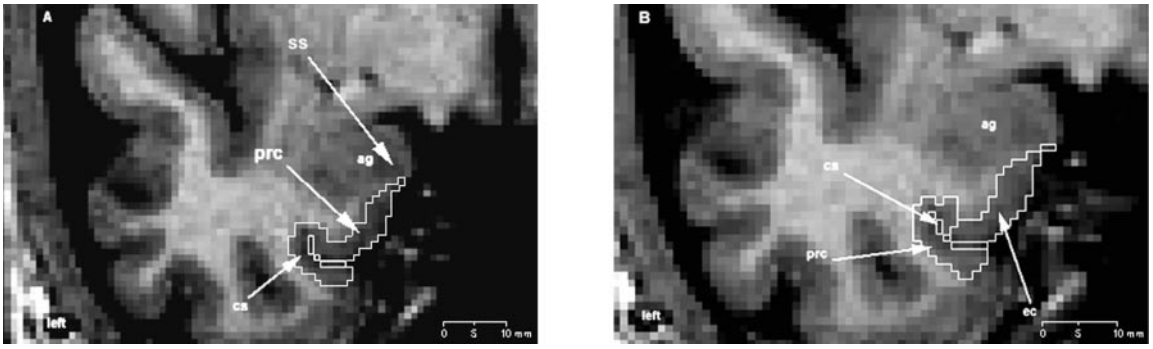

Figure 5. Segmentation of the PRC. In the cases where the collateral sulcus stretched further anterior than the FTJ, the first appearance of the CS marked the rostral extreme of the PRC (*A*). The EC in these cases was considered to start 2 mm posterior to the first appearance of the CS. The PRC extended from the point where an imaginary extension of the white matter superior to it would touch the pial MTL surface. In cases where the FTJ was located anterior to the first appearance of the CS in the coronal orientations, the CS began 1 mm anterior to the appearance of the FTJ. In these cases, the first appearance of the CS marked the rostral extreme of the EC, and the PRC extended from the midpoint of the medial bank of the CS to the edge of its lateral bank (*B*).

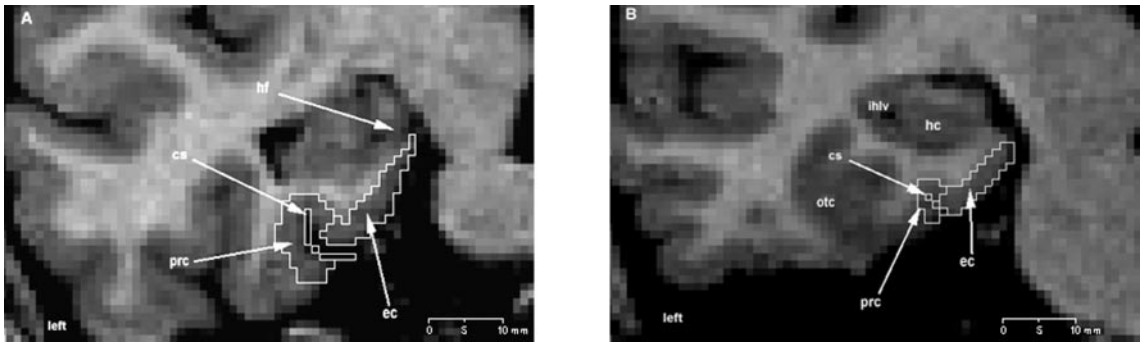

Figure 6. Segmentation of EC. The EC was chosen to always extend to the midpoint of the medial bank of the first appearing CS, independent of the depth of this sulcus (*A*). The lateral border was chosen as hippocampal fissure, sulcus seminannularis, or an extension of the superior white matter border of the EC if the latter two were poorly visible (see Fig. 5 legend and text). In cases where the CS was interrupted or very shallow, a reduction of the corresponding volumes of EC and PRC could be observed (*B*).

cerebrospinal fluid (CSF), or gray matter and durae marked the border of the EC (Fig. 5*B*). In cases where it was suspected that a layer of durae was present between the medial end of the EC and CSF, this classification was confirmed in both transverse views and the tissue was excluded from all measurements.

Further caudally, the hippocampus started to appear and defined the superolateral border of the EC (Fig. 6*A*). Notably, the subiculum was excluded from the measurements, thus allowing for a small section not to be labeled in the transition between hippocampus and EC (Pruessner *et al*., 2000). By using these neuroanatomical definitions, we included the presubiculum and parasubiculum in the volume of EC anteriorly. More posteriorly, it was included in the volume of the PHC (see below). Following the hippocampus further caudally, the disappearance of the gyrus intralimbicus and the hippocampal fissure could usually be observed distinctively in coronal images (Fig. 6*B*). This landmark was employed to define the caudal end of the EC. The EC was considered to end 2 mm posterior to the coronal image on which the gyrus intralimbicus disappeared. Posterior to this location, the EC was briefly replaced by the PRC, which continued for another 2 mm. From this point on to the posterior end of the hippocampus, it was replaced completely by PHC.

Segmentation of the PHC

At its rostral end, the superior and inferior borders of the PHC were identical to those of the PRC in more rostral sections. It extended from the inferior border of the hippocampus to the lateral edge of the CS. If two CS were present, then the PHC extended to the fundus of the more lateral CS. Following the PHC along its rostrocaudal extent, the appearance of the calcarine sulcus was usually observed at the level of the hippocampal tail. If this sulcus was present, the superior border of the PHC was defined at its inferior edge. The ventral border of the PHC remained identical to that of the PRC, so that it also extended to the edge of the lateral bank of the CS. If two CS were present, the PHC extended to the fundus of the more laterally located CS. The same border definitions could be applied when moving more caudally in coronal images from the hippocampal body to the hippocampal tail (Fig. 7*A*). Segmentation of the PHC continued on coronal images on which the ovoid mass of gray matter of the hippocampal tail was attached to the trigone of the lateral ventricle (Fig. 7*B*). The caudal end of the PHC was defined to be at the level at which the gray matter mass of the hippocampus disappeared in the coronal views entirely. This border was chosen somewhat arbitrarily because no corresponding anatomical landmarks have been reported for the posterior end of the PHC in histological studies so far.

Reliability and Validity Assessment

Three MR acquisitions were randomly selected from the 40 subjects for analysis of interrater reliability. In these three MR acquisitions, MTL structures of the current protocol were segmented by three different raters; interrater reliability coefficients were calculated assuming that the three raters were the only raters of interest (Shrout and Fleiss, 1979). For the purpose of calculating intrarater reliability coefficients, one of the three raters (J.C.P.) labeled all structures of the MTL from this protocol in five subjects five subsequent times, with at least 1 week elapsing between consecutive segmentations. All raters were blind with regard to age and sex of the subjects, but not to hemisphere. For validation purposes, the mean volumes from the current protocol were compared to the mean values reported in the protocol by Insausti *et al.* (Insausti *et al.*, 1998) for EC and PRC, because borders for segmentation of these structures are identical in both protocols with only minor exceptions (affecting the TPC and the EC/PRC transition on the medial bank of the CS). Volumes were also compared for the TPC, although differences between protocols were more substantial (see below).

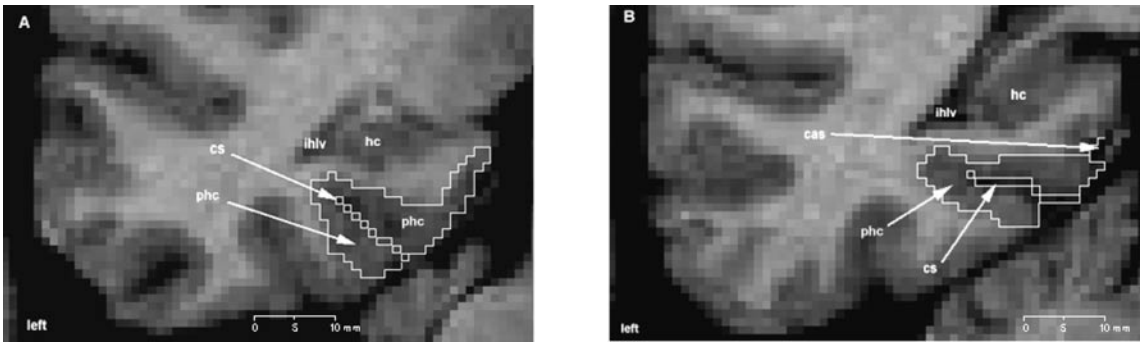

Figure 7. Segmentation of PHC. Posterior to the gyrus intralimbicus, the EC and PRC are replaced by the PHC. The rules for the medial and lateral borders are identical to the rules for segmentation of the PRC when no EC is present (*A*). When visible, the calcarine sulcus (cas) was chosen as the medial border (*B*).

Statistical Analyses including Examination of Sex and Age Effects
Descriptive statistics for the measured structures were calculated across all subjects and included minimum and maximum volumes, as well as means and standard deviations. To allow for an estimation of possible effects of sex on the MTL volumes, descriptive statistics were also calculated separately for the groups of men and women. In order to test for effects of sex on the MTL volumes statistically, two-way mixed design analyses of variance (ANOVA; sex by hemisphere) were calculated, with the volumes of the MTL as dependent variables. In addition, Pearson correlations were computed for the analysis of the association between age and structure size in both sex groups. In order to test whether the anatomical variability of the collateral sulcus had an effect on the statistical calculations for age and sex relationships, the volumes of the MTL structures were also corrected for the parts of the CS that were adjacent to the respective structures in each hemisphere and the above statistical tests were then rerun with these corrected volumes (except for the TPC, which is located anterior to the CS). This procedure was performed to investigate whether the abundance of variation in CS anatomy might mask sex differences, or associations of the MTL volumes with age. For the correction, the CS was segmented according to the guidelines described above. Since the CS was consistently labeled as having the width of 1 voxel, the resulting volume can be regarded as standardized surface area. The surface area of the CS was calculated separately for the two hemispheres and separately for the corresponding segments of the overlying gray matter structures. Thus, CS surfaces areas could be computed for the left entorhinal/perirhinal area, left parahippocampal area, right entorhinal/perirhinal area and right parahippocampal area. The volumes of the measured MTL structures were then corrected for CS variability by computing a ratio between the volume of MTL structure and the corresponding CS standardized surface area.

The power of all statistical tests was calculated, according to the formulas provided by Cohen (Cohen, 1988). In the case of significant results, the effect sizes were calculated to provide an estimate of the strength of the reported findings. In the case of insignificant results, the power calculations allowed for an estimation of the probability of finding an effect in a sample of the current size, assuming the effect existed in the general population.

Results

The reliability measurements for intra- and interrater calculations are shown in Table 2. The differences between the three raters were small and ranged from 3 (left PHC) to 8% (right TPC). The intrarater variability was also very limited, ranging from 2.5 (left PHC) to 6% (left TPC). Minimum and maximum volumes of PHG structures, mean values and standard errors of mean are shown in Table 3, separately for left and right hemisphere. Data are presented for the total group, and for women and men separately. The comparison of these values with those reported by Insausti *et al* (Insausti *et al.*, 1998) shows different results depending on the structure. The mean values for EC and PRC show good accordance between protocols (left EC – this study 1738 mm^3, Insausti 1510 mm^3; right EC – this study 1745 mm^3, Insausti 1645 mm^3; left PRC – this study 2485 mm^3, Insausti 2585 mm^3; right PRC – this study 2416 mm^3, Insausti 2577 mm^3). For the TPC, however, the results from our study suggest a higher volume (5838 and 6308 mm^3 for left and right TPC, respectively) when compared to the mean volumes reported by Insausti (3421 versus 3228 mm^3 for left and right TPC, respectively). This is somewhat surprising when considering that we chose to concentrate on the medial portion of the TPC only. This comparison indicates a considerable difference in the assessment of the TPC between the two protocols, especially in light of the good accordance obtained for the other structures. The mean age of their younger control group (age range 21–43 years) matches well with the control group investigated in the present study (age range 18–42 years) and thus can not be at the origin of these differences. Also, the comparison is restricted to the uncorrected values because Insausti *et al*. did not perform a correction for variability of the CS shape.

Table 2
Intra- and interrater intraclass reliability coefficients

	Intra		Inter	
	Left	Right	Left	Right
CS	0.90	0.91	0.88	0.89
TPC	0.86	0.87	0.92	0.84
PRC	0.94	0.92	0.90	0.92
EC	0.96	0.91	0.95	0.93
PHC	0.93	0.91	0.90	0.88

Interrater correlations were obtained from three subjects analyzed independently by three different raters; intrarater correlations were obtained from five subjects analyzed five times by the same rater with 1 month interval between ratings.

Of further interest is the comparison of the variability found in the uncorrected structures between the two protocols, which is performed best using the coefficients of variation. Here, the two protocols show good accordance, with the current protocol producing coefficients in the range from 0.11 to 0.31 (uncorrected values), while the Insausti protocol produced coefficients of variation in the range from 0.11 to 0.37.

For the corrected values, it is of interest to note that the coefficients of variation decrease sharply for the PRC, while they seem to increase for ERC and PHG; the TPC does not yield corrected values since it does not lie adjacent to the CS.

The two-factor mixed design ANOVA (sex by hemisphere) for all structures showed no effects of sex on the uncorrected volumes of TPC, PRC, PHC, or EC (all $F < 1$, $P > 0.20$). With regard to hemispheric differences, no effects were observed for PRC ($F < 1$, $P > 0.30$), while a trend could be observed for the

Table 3
Mean, SD, minimum and maximum, and coefficient of variation for all structures, separated for gender and hemisphere

	TPC	PRC	EC	PHC	PRC_CS	EC_CS	PHC_CS
All left ($n = 40$)							
Mean	6224	2502	1553	2675	0.91	7.062	13.622
SD	1550	724	402	489	0.023	2.58	3.59
Minimum	3467	1592	1008	1243	0.845	2.76	5.87
Maximum	9131	4187	2804	3608	0.952	12.832	21.64
CV	0.25	0.29	0.26	0.18	0.025	0.37	0.26
All right ($n = 40$)							
Mean	6913	2417	1672	2469	0.905	7.159	12.74
SD	1811	620	364	310	0.023	2.29	3.54
Minimum	4133	1512	729	1772	0.851	3.667	5.77
Maximum	10 546	3748	2573	3238	0.95	12.73	24.27
CV	0.26	0.26	0.22	0.13	0.02	0.32	0.28
Women left ($n = 20$)							
Mean	6570	2415	1684	2810	0.904	7.123	13.5
SD	1437	696	306	445	0.019	2.06	3.53
Minimum	3900	1601	1273	2083	0.86	3.082	9.42
Maximum	8663	4019	2197	3608	0.93	9.72	18.99
CV	0.21	0.29	0.19	0.16	0.02	0.29	0.26
Women right ($n = 20$)							
Mean	6868	2456	1818	2454	0.903	7.76	13.46
SD	2006	631	204	358	0.026	2.74	4.31
Minimum	4133	1512	1298	1772	0.85	4.37	7.88
Maximum	10 546	3748	1996	3238	0.94	12.73	24.27
CV	0.29	0.26	0.11	0.15	0.03	0.35	0.32
Men left ($n = 20$)							
Mean	5979	2577	1441	2559	0.915	7.01	13.73
SD	1623	765	451	511	0.027	3.03	3.77
Minimum	3467	1592	1008	1243	0.845	2.769	5.87
Maximum	9131	4187	2804	3066	0.952	12.83	21.65
CV	0.27	0.30	0.31	0.20	0.03	0.43	0.32
Men right ($n = 20$)							
Mean	6945	2385	1547	2481	0.91	6.641	12.13
SD	1724	631	428	275	0.021	1.77	2.75
Minimum	4322	1560	729	2077	0.869	3.667	5.77
Maximum	9840	3673	2573	2958	0.954	10.45	17.24
CV	0.25	0.26	0.28	0.11	0.02	0.27	0.23

All values are given in mm^3. CS, collateral sulcus; TPC, temporopolar cortex; PRC, perirhinal cortex; EC, entorhinal cortex; PHC, parahippocampal cortex; PRC_CS, EC_CS, PHC_CS, perirhinal, entorhinal and parahippocampal cortex corrected for the variability of the collateral sulcus; CV, coefficient of variance.

TPC ($F = 2.46$, $P = 0.07$) and the EC ($F = 2.55$, $P = 0.06$) with right-sided structures showing higher volumes than left-sided ones. The ANOVA performed on the PHC volumes indicated significant differences between left and right hemisphere ($F = 5.2$, $P = 0.01$). A Scheffe *post hoc* test indicated that the left PHC was larger than the right in both men and women. No interaction effect was significant (all $F < 1$, $P > 0.20$).

For the corrected volumes, no effect of sex or hemisphere was found for EC (both $F < 1$, $P > 0.20$), PRC (sex, $F < 1$, $P > 0.20$; hemisphere, $F = 1.4$, $P > 0.20$), or PHC ($F < 1$). Also, no significant interaction effect could be observed (all $F < 1$, $P > 0.20$). The results from Pearson correlations between age and the corrected and uncorrected MTL structure volumes of the left and right hemisphere are shown in Table 4, calculated separately for men and women. Considering the results from the uncorrected volumes, with the exception of the right PRC in the group of women ($r = 0.60$, $P = 0.001$), no significant correlation was observed. This pattern changed considerably when the results from the corrected MTL structures were examined. While the former positive significant correlation between age and volume for the right PRC in the group of women disappeared, two significant correlations with age emerged in the group of men: the volumes of the right EC and the left PHC were significantly negatively correlated with age ($r = -0.50$ and $r = -0.48$, respectively, both $P < 0.05$). In addition, there was a negative correlation of age with the left TPC in the group of men ($r = -0.60$, $P < 0.01$; only uncorrected volumes available). Together, these results suggest an association between parts of the left and right PHG volume and age in the group of men. It should be noted, however, that none of these correlations exceed statistical threshold when corrections for multiple comparisons in this set of calculations were performed.

Table 4
Pearson correlation between age and volume of the uncorrected and corrected MTL structures in the 40 subjects of this study, calculated separately for men and women

	Women ($n = 20$)		Men ($n = 20$)	
	Left	Right	Left	Right
PRC	0.35	**0.60**	–0.22	0.37
	$P = 0.09$	***P* < 0.01**	n.s.	n.s.
EC	0.03	0.38	–0.08	0.33
	n.s.	$P = 0.07$	n.s.	n.s.
PHC	–0.05	0.05	0.23	0.16
	n.s.	n.s.	n.s.	n.s.
TPC	–0.34	–0.23	**–0.60**	–0.24
	$P = 0.09$	n.s.	***P* < 0.01**	n.s.
PRC_CS	0.15	0.27	0.32	–0.03
	n.s.	n.s.	n.s.	n.s.
EC_CS	–0.17	–0.01	0.25	**–0.50**
	n.s.	n.s.	n.s.	***P* < 0.03**
PHC_CS	–0.20	–0.21	**–0.48**	–0.27
	n.s.	n.s.	***P* < 0.04**	n.s.

Computation of the power of the tests for possible effects of age, hemisphere or gender on the respective volumes revealed $\lambda = 13$. With the α-level set to 0.05, the chance of finding an existing population effect in the selected subjects was $t = 0.95$, assuming a medium effect size of $f^2 = 0.25$. With a smaller effect size of $f^2 = 0.10$, the chance of revealing a significant difference in this group of subjects, given an existing population effect, would have dropped to $t = 0.50$. The reported difference in PHC volumes between the left and right hemisphere corresponded to an effect size of $f^2 = 0.11$, thus an estimated 10% of variability in parahippocampal measures was explained by the hemisphere alone ($\omega^2 = 0.10$). For the significant correlations between age and PRC and EC volumes in the left hemisphere, the size of the correlations suggests that ~17% of the variability found in the entorhinal and perirhinal cortex measures is explained by the age of the subjects in the group of men.

Discussion

This paper presents a new segmentation protocol for the volumetric assessment of the major MTL structures that constitute the PHG. It was developed in direct succession to segmentation guidelines previously published by this laboratory for the assessment of hippocampus and amygdala (Pruessner *et al.*, 2000), allowing for measurement of all major MTL structures in an integrated manner with consistent neuroanatomical definitions. The protocol employed 3D-analysis software that enables the user to choose the viewing angle for MR images freely in any orientation, thereby effectively addressing some of the previous concerns regarding orientation in conjunction with segmentation of MTL structures (de Leon *et al.*, 2001). An additional emphasis was put on taking into consideration the neuroanatomical variability of the CS across different individuals. The boundaries and neuroanatomical definitions used for segmentation of the TPC, PRC and EC were adopted from those presented by Insausti *et al* (Insausti *et al.*, 1998), which were derived from a combined analysis of histological and MR data. The anatomical guidelines for segmentation of the parahippocampal cortex were chosen in accordance with Van Hoesen's suggestions (Van Hoesen *et al.*, 2000).

The results of the intra- and intrarater reliability calculations indicate that the present guidelines provide a reliable and precise tool to segment and measure the irregularly shaped MTL structures. Comparing the current results with those from a previously published study with similar segmentation guidelines (Insausti *et al.*, 1998) revealed good accordance between the volumes of these structures, with the exception of the TPC, which appeared larger in the current protocol. This is surprising because we chose to concentrate on the medial aspect of the TPC only, whereas the previously published protocol assessed the TPC in its entire extent. Future investigations will be necessary to verify mean volumes for this structure in other samples of normal controls.

As compared to previously published segmentation protocols for the volumetric assessment of MTL structures in the PHG, the current approach differs from past studies in several aspects. First, the presented guidelines allow segmentation of all cortices surrounding the hippocampus and amygdala, except for the small portion that consists of pyriform cortex, and subiculum; thus, it covers the majority of gray-matter structures constituting the PHG. Most of the available protocols for segmentation of MTL structures other than the hippocampus have focused on the EC exclusively and thus do not allow for a comparison of different MTL structures. Being able to investigate these structures within a unified protocol provides a clear advantage for testing the possible involvement of different PHG cortices in aging or neurodegenerative processes and for localizing MTL activations in functional neuroimaging studies. Secondly, the current protocol employs improved visualization tools to measure precisely volumes of PRC, EC and PHC. To illustrate the point, it is worthwhile considering the current debate about the usefulness of EC segmentation protocols in relation to specific disease processes (Xu *et al.*, 2000), which directly relates to this issue. While it is commonly acknowledged across laboratories that the MTL structures surrounding the hippocampus (especially the EC) are first affected by the onset of Alzheimer's disease (and possibly also by other neurodegenerative diseases), segmentation protocols presenting guidelines for the assessment of these structures have failed to produce superior results when compared to those assessing only the hippocampus. This has been attributed to problems in visualization and delineation of the boundaries of the respective MTL structures, mostly the EC (Insausti *et al.*, 1998; de Leon *et al.*, 2001); it has been argued that the difficulties in consistently delineating the anterior and superomedial borders of the EC are responsible for the poor results. The software used for this protocol enables researchers to overcome this problem by allowing free definition of the viewing angle that allows realignment of the MR images along the CS. Thus, it allows for precise identification of cortex boundaries by revealing the sulcal patterns in a superior manner. Thirdly, the current protocol suggests a method of correcting for the anatomical variability found in the CS and thus the surrounding cortices. Lack of correction for anatomical variability has likely contributed to inconsistent results with EC segmentation in the past. In most of the available segmentation guidelines, the inferolateral border of the EC is defined in reference to the medial bank of the first appearing CS. In some protocols, the lateral border of the EC varies with the depth of the CS (Insausti *et al.*, 1998), while other approaches define the lateral border of the EC at the medial lip of the first appearing CS (Bernasconi *et al.*, 1999; Chan *et al.*, 2001). In the present protocol, by contrast, the midpoint of the medial bank of the first appearing CS was chosen as the consistent lateral transition between EC and PRC. As a consequence, interruptions, side-branches, or variations in the depth of the CS will have a direct impact on EC and PRC volumes that need to be considered when interpreting these volumes.

In the 40 subjects segmented in this study, a double-branched CS was found in ~35% of subjects. Interruptions of the CS were apparent in ~20% of subjects. These variations of the CS can be expected to have a significant impact on the volume of the structures surrounding the CS (i.e. EC, PRC and PHC). Figure 8 provides examples of these variations and the consequences for the resulting shape and volume of the surrounding structures. In the upper row, an uninterrupted, non-side-branched collateral sulcus is shown, which fulfills the requirements for a homogeneous EC, PRC and PHC segmentation. As can be appreciated from the investigation of the middle (interrupted CS) and lower (double-branched CS) rows, anatomical variations then can be expected significantly to modify the resulting volume of the structures surrounding the CS. The most dramatic effect to result from an interruption or a side branch of the CS can be expected to occur on the volume of the PRC. However, the EC will also be affected, since an interruption of the CS will result in a smaller amount of gray matter to be included in the inferolateral part of the EC.

By calculating the ratio of cortex to standardized sulcus surface area, these anatomical variations can be taken into account. Variations in the depth of the sulcus, as well as side

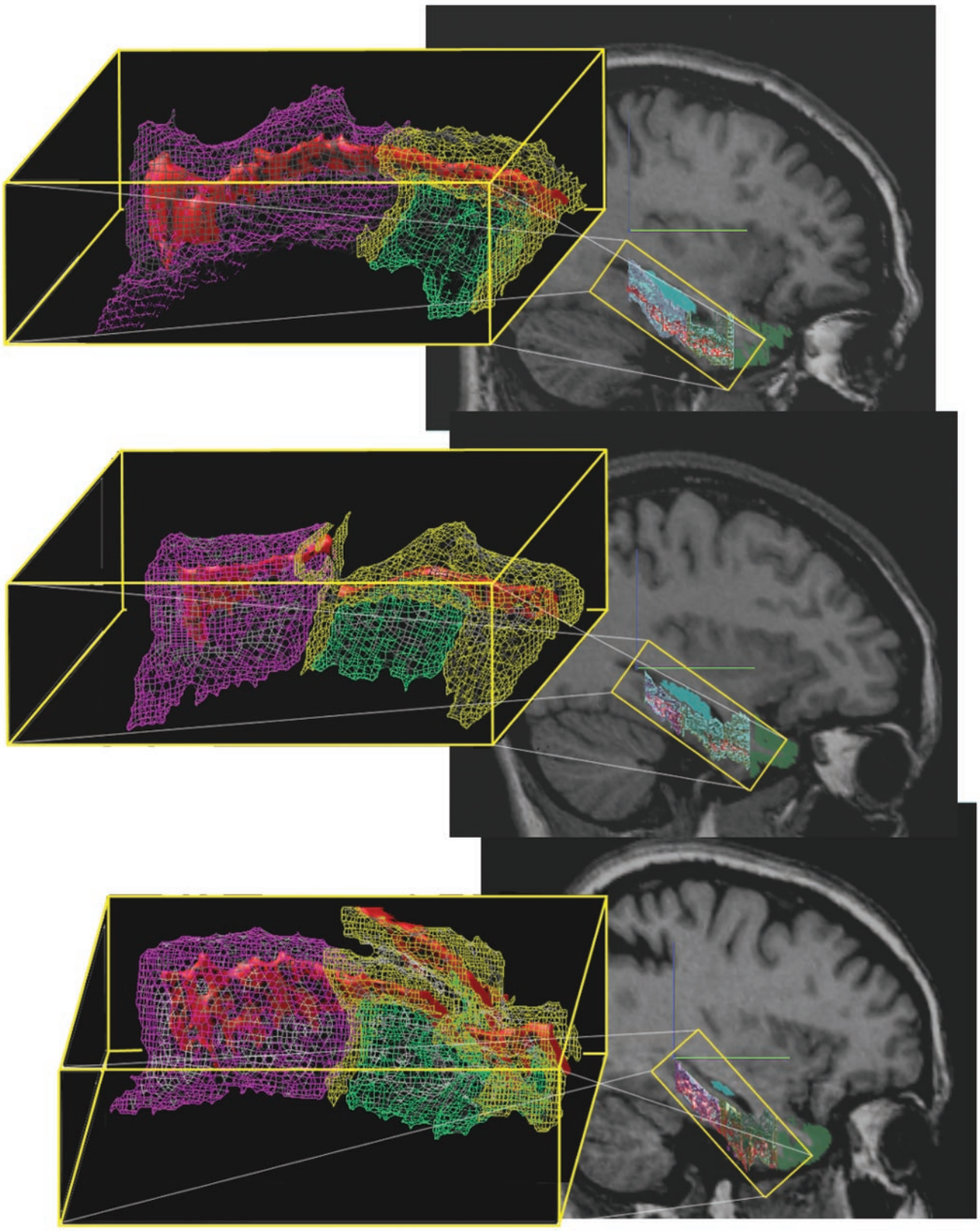

Figure 8. Effect of anatomical variation of the MTL on the volumes of EC, PRC and PHC. Three anatomical variations of MTL lobe anatomy are shown, with an uninterrupted, non-side-branched CS shown in the upper row, an interrupted CS shown in the middle row and a side-branched CS shown in the lower row. For better visualization, corresponding segments of the CS were cut out from the MR image and underwent 3D rendering. The CS is shown in solid red in all examples. The surrounding gray matter structures are rendered as mesh wire around the CS. PRC is displayed in yellow, EC is shown in green and PHC is displayed in pink. An interruption of the CS will have an effect of reduction on the volumes of PRC and EC, as can be seen when comparing the upper and the middle row. A side branch of the CS will cause the volume of the PRC to be enlarged, as can be seen when comparing the upper and the lower rows. By computing a cortex-to-CS ratio (possible after segmenting the CS itself), the volumes of the gray matter structures surrounding the CS can be corrected for anatomical variations of the CS.

branches and interruptions of the CS will no longer add to the heterogeneity within a group of subjects. The effects of the correction were demonstrated in the current study when considering the changes in the age-related correlational pattern with the corrected and uncorrected volumes of PRC, EC and PHC. Associations with age emerged only for the corrected volumes, suggesting that the correction made it possible to derive additional information about the measured MTL structures. It seems likely that by correcting for differences in anatomical shape across subjects, as performed by calculating a 'cortex to standardized sulcus surface area' ratio, cortical thickness becomes a more dominant factor in determining the volume of individual MTL structures. Thus, the emerging correlations with age might reflect this stronger reference to cortical thickness. Our interpretation is in line with current findings on age-related changes in other parts of the brain, where men have been reported to undergo stronger changes than women (Blatter *et al.*, 1995; Coffey *et al.*, 1998). Recently, we have shown that the hippocampi in a larger sample of subjects, including those tested here, showed a sex-specific reduction of volume for both left and right hippocampus in the same correlation range (Pruessner *et al.*, 2001). Therefore, it is of interest to see a trend for sex differences in the same direction emerging for other MTL structures as well.

A note of caution is required when considering the coefficients of variation of the corrected and uncorrected MTL volumes. While the variability of the PRC is reduced considerably after correcting for the CS surface areas, the coefficients of variation for the EC and PHC actually seem to increase. This finding can be interpreted as showing that the PRC variability is mostly determined by the variability found in the CS, but it suggests at the same time that additional factors influence the heterogeneity of EC and PHC. This conclusion receives support from the observation that EC and PHC are only partly determined by the actual shape of the CS and partly by the shape of the medial part of the MTL surface. Thus, it appears necessary to investigate both the uncorrected and the corrected volumes of MTL structures to obtain all relevant information about the volume of the different PHG cortices. The analysis of the corrected volumes may add further information when investigating changes occurring in the MTL in association with sociodemographic or clinical variables. Future studies need to determine whether the abundant anatomical variability found in the CS – and consequently also in EC, PRC and PHC – is associated with specific functional consequences as well.

With regard to hemispheric differences, results were inconsistent in the current study across different structures, with the uncorrected volumes of TPC and EC showing a trend to be larger in the right hemisphere, and the PHC being significantly larger in the left hemisphere. However, these differences disappeared when taking into account the variability of the CS. Recent studies investigating hippocampal volume differences across hemispheres consistently found the right hippocampus to be larger than the left (Watson *et al.*, 1992; Mori *et al.*, 1997; Csernansky *et al.*, 1998; Pruessner *et al.*, 2000). In the study by Insausti *et al*. (Insausti *et al.*, 1998), EC volume was also found to be greater in the right than in the left hemisphere. At present, it is unclear whether the discrepancy in the results for the EC between the current study and that by Insausti is due to the differences in the protocols employed or to differences in the sample examined. Further studies are needed to investigate hemispheric differences across all MTL structures in the same sample.

In summary, the protocol presented in this manuscript allows for the precise segmentation of the temporopolar, entorhinal, perirhinal and parahippocampal cortex. It is directly compatible with a previously published protocol for the volumetric assessment of the hippocampus and amygdala (Pruessner *et al.*, 2000), allowing for the examination of all major MTL structures with consistent anatomical definitions. The intraclass intra- and interrater reliability coefficients reported here are comparable to those from other studies describing segmentation protocols for the MTL structures (Honeycutt *et al.*, 1998; Killiany *et al.*, 2000; Xu *et al.*, 2000). The described method of calculating a standardized surface area of the CS allows for correcting of the cortical volumes for anatomical variability of the adjacent CS. We propose that the segmentation guidelines presented here provide a powerful tool to investigate the involvement of all major MTL structures in normal aging and in neurodegenerative processes, and to help with the localization of MTL activations in functional neuroimaging research.

Notes

This work was supported by a NARSAD grant to J.C.P. and a NSERC grant to S.K.

Address correspondence to Dr Jens C. Pruessner, McConnell Brain Imaging Center, Montreal Neurological Institute, 3801 University Street, Montreal, Canada H3A 2B4. Email: jens@bic.mni.mcgill.ca.

References

Aggleton JP, Brown MW (1999) Episodic memory, amnesia and the hippocampal/anterior thalamic axis. Behav Brain Sci 22:425–498.

Amaral DG, Insausti R (1990) Hippocampal formation. In: The human nervous system (Paxinos G, ed.), pp. 711–755. San Diego, CA: Academic Press.

Baron JC, Chetelat G, Desgranges B, Perchey G, Landeau B, de la Sayette V, Eustache F (2001) *In vivo* mapping of gray matter loss with voxel-based morphometry in mild alzheimer's disease. Neuroimage 14:298–309.

Barta PE, Powers RE, Aylward EH, Chase GA, Harris GJ, Rabins PV, Tune LE, Pearlson GD (1997) Quantitative MRI volume changes in late onset schizophrenia and Alzheimer's disease compared to normal controls. Psychiatry Res 68:65–75.

Bernasconi N, Bernasconi A, Andermann F, Dubeau F, Feindel W, Reutens DC (1999) Entorhinal cortex in temporal lobe epilepsy: a quantitative MRI study. Neurology 52:1870–1876.

Bernasconi N, Bernasconi A, Caramanos Z, Andermann F, Dubeau F, Arnold DL (2000) Morphometric MRI analysis of the parahippocampal region in temporal lobe epilepsy. Ann NY Acad Sci 911:495–500.

Bernasconi N, Bernasconi A, Caramanos Z, Dubeau F, Richardson J, Andermann F, Arnold DL (2001) Entorhinal cortex atrophy in epilepsy patients exhibiting normal hippocampal volumes. Neurology 56:1335–1339.

Blatter DD, Bigler ED, Gale SD, Johnson SC, Anderson CV, Burnett BM, Parker N, Kurth S, Horn SD (1995) Quantitative volumetric analysis of brain MR: normative database spanning 5 decades of life. American Journal of Neuroradiology 16:241–251.

Cabeza R, Nyberg L (2000) Imaging cognition II: an empirical review of 275 PET and fMRI studies. J Cogn Neurosci 12:1–47.

Chan D, Fox NC, Scahill RI, Crum WR, Whitwell JL, Leschziner G, Rossor AM, Stevens JM, Cipolotti L, Rossor MN (2001) Patterns of temporal lobe atrophy in semantic dementia and Alzheimer's disease. Ann Neurol 49:433–442.

Coffey CE, Lucke JF, Saxton JA, Ratcliff G, Unitas LJ, Billig B, Bryan RN (1998) Sex differences in brain aging: a quantitative magnetic resonance imaging study. Arch Neurol 55:169–179. [Published erratum appears in Arch Neurol 1998;55:627.]

Cohen J (1988) Statistical power analysis for the behavioral sciences, 2nd edn. Hillsdale, NJ: Erlbaum.

Collins DL, Neelin P, Peters TM, Evans AC (1994) Automatic 3D intersubject registration of MR volumetric data in standardized Talairach space. J Comput Assist Tomogr 18:192–205.

Csernansky JG, Joshi S, Wang L, Haller JW, Gado M, Miller JP, Grenander U, Miller MI (1998) Hippocampal morphometry in

schizophrenia by high dimensional brain mapping. Proc Natl Acad Sci USA 95:11406–11411.
de Leon MJ, Convit A, DeSanti S, Bobinski M, George AE, Wisniewski HM, Rusinek H, Carroll R, Saint Louis LA (1997) Contribution of structural neuroimaging to the early diagnosis of Alzheimer's disease. Int Psychogeriatr 9(Suppl. 1):183–190; discussion 247–152.
de Leon M, Bobinski M, Convit A, Wolf O, Insausti R (2001) Usefulness of MRI measures of entorhinal cortex versus hippocampus in AD. Neurology 56: 820–821.
Double KL, Halliday GM, McRitchie DA, Reid WG, Hely MA, Morris JG (1996) Regional brain atrophy in idiopathic Parkinson's disease and diffuse Lewy body disease. Dementia 7:304–313.
Eichenbaum H, Otto T, Cohen NJ (1994) Two functional components of the hippocampal memory systems. Behav Brain Sci 17:449–581.
Gabrieli JD, Brewer JB, Desmond JE, Glover GH (1997) Separate neural bases of two fundamental memory processes in the human medial temporal lobe. Science 276:264–266.
Giedd JN, Snell JW, Lange N, Rajapakse JC, Casey BJ, Kozuch PL, Vaituzis AC, Vauss YC, Hamburger SD, Kaysen D, Rapoport JL (1996a) Quantitative magnetic resonance imaging of human brain development: ages 4–18. Cereb Cortex 6:551–560.
Giedd JN, Vaituzis AC, Hamburger SD, Lange N, Rajapakse JC, Kaysen D, Vauss YC, Rapoport JL (1996b) Quantitative MRI of the temporal lobe, amygdala, and hippocampus in normal human development: ages 4–18 years. J Comp Neurol 366:223–230.
Honeycutt NA, Smith PD, Aylward E, Li Q, Chan M, Barta PE, Pearlson GD (1998) Mesial temporal lobe measurements on magnetic resonance imaging scans. Psychiatry Res 83:85–94.
Insausti R, Juottonen K, Soininen H, Insausti AM, Partanen K, Vainio P, Laakso MP, Pitkanen A (1998) MR volumetric analysis of the human entorhinal, perirhinal, and temporopolar cortices. Am J Neuroradiol 19: 659–671.
Kesslak JP, Nalcioglu O, Cotman CW (1991) Quantification of magnetic resonance scans for hippocampal and parahippocampal atrophy in Alzheimer's disease. Neurology 41:51–54.
Killiany RJ, Gomez-Isla T, Moss M, Kikinis R, Sandor T, Jolesz F, Tanzi R, Jones K, Hyman BT, Albert MS (2000) Use of structural magnetic resonance imaging to predict who will get Alzheimer's disease. Ann Neurol 47:430–439.
Krasuski JS, Alexander GE, Horwitz B, Daly EM, Murphy DG, Rapoport SI, Schapiro MB (1998) Volumes of medial temporal lobe structures in patients with Alzheimer's disease and mild cognitive impairment (and in healthy controls). Biol Psychiatry 43:60–68.
Mazziotta JC, Toga AW, Evans A, Fox P, Lancaster J (1995) A probabilistic atlas of the human brain: theory and rationale for its development. The International Consortium for Brain Mapping (ICBM). Neuroimage 2:89–101.
Mori E, Yoneda Y, Yamashita H, Hirono N, Ikeda M, Yamadori A (1997) Medial temporal structures relate to memory impairment in Alzheimer's disease: an MRI volumetric study. J Neurol Neurosurg Psychiatry 63:214–221.
Pruessner JC, Li LM, Serles W, Pruessner M, Collins DL, Kabani N, Lupien S, Evans AC (2000) Volumetry of hippocampus and amygdala with high-resolution MRI and three-dimensional analysis software: minimizing the discrepancies between laboratories. Cereb Cortex 10:433–442.
Pruessner J, Collins D, Pruessner M, Evans A (2001) Age and gender predict volume decline in the hippocampus in healthy males in early adulthood. J Neurosci. 21:194–200.
Schacter DL, Wagner AD (1999) Medial temporal lobe activations in fMRI and PET studies of episodic encoding and retrieval. Hippocampus 9:7–24.
Scoville WB, Milner B (2000) Loss of recent memory after bilateral hippocampal lesions. J Neuropsychiatry Clin Neurosci 12:103–113.
Shrout PE, Fleiss JL (1979) Intraclass correlations: uses in assessing rater reliability. Psychol Bull 86:420–428.
Sled JG, Zijdenbos AP, Evans AC (1998) A nonparametric method for automatic correction of intensity nonuniformity in MRI data. IEEE Trans Med Imaging 17:87–97.
Stark CE, Squire LR (2001) Simple and associative recognition memory in the hippocampal region. Learn Mem 8:190–197.
Talairach J, Tournoux P (1988) Co-planner stereotactic atlas of the human brain; 3-dimensional proportional system: an approach to cerebral imaging. New York: Thieme.
Van Hoesen GW, Augustinack JC, Dierking J, Redman SJ, Thangavel R (2000) The parahippocampal gyrus in Alzheimer's disease. Clinical and preclinical neuroanatomical correlates. Ann NY Acad Sci 911: 254–274.
Watson C, Andermann F, Gloor P, Jones-Gotman M, Peters T, Evans A, Olivier A, Melanson D, Leroux G (1992) Anatomic basis of amygdaloid and hippocampal volume measurement by magnetic resonance imaging. Neurology 42:1743–1750.
Xu Y, Jack CR Jr, O'Brien PC, Kokmen E, Smith GE, Ivnik RJ, Boeve BF, Tangalos RG, Petersen RC (2000) Usefulness of MRI measures of entorhinal cortex versus hippocampus in AD. Neurology 54: 1760–1767.